PCCP



PAPER View Article Online
View Journal | View Issue



Cite this: Phys. Chem. Chem. Phys., 2021, 23, 5834

Received 12th January 2021, Accepted 4th March 2021

DOI: 10.1039/d1cp00167a

rsc.li/pccp

Adsorption and reaction pathways of 7-octenoic acid on copper†

Robert Bavisotto, Resham Rana, Nicholas Hopper, Dustin Olson and Wilfred T. Tysoe **

The surface structure and reaction pathways of 7-octenoic acid are studied on a clean copper substrate in ultrahigh vacuum using a combination of reflection—absorption infrared spectroscopy, X-ray photoelectron spectroscopy, temperature-programmed desorption and scanning-tunneling microscopy, supplemented by first-principles density functional theory calculations. 7-Octenoic acid adsorbs molecularly on copper below $\sim\!260$ K in a flat-lying configuration at low coverages, becoming more upright as the coverage increases. It deprotonates following adsorption at $\sim\!300$ K to form an η^2 -7-octenoate species. This also lies flat at low coverages, but forms a more vertical self-assembled monolayer as the coverage increases. Heating causes the 7-octenoate species to start to tilt, which produces a small amount of carbon dioxide at $\sim\!550$ K and some hydrogen in a peak at $\sim\!615$ K ascribed to the reaction of these tilted species. The majority of the decarbonylation occurs at $\sim\!650$ K when CO₂ and hydrogen evolve simultaneously. Approximately half of the carbon is deposited on the surface as oligomeric species that undergo further dehydrogenation to evolve more hydrogen at $\sim\!740$ K. This leaves a carbonaceous layer on the surface, which contains hexagonal motifs connoting the onset of graphitization of the surface.

1. Introduction

Self-assembled monolayers (SAMs) have been used for a wide range of applications^{1–5} from chemical anchors to nanoparticles for drug delivery,⁶ to being used as sensors,⁷ for molecular electronics,^{8–12} or for preventing adhesion in micro-electromechanical system (MEMS).^{13,14} SAMs comprise a surface anchoring group, often a thiol,^{2,4,15–19} and a long-chain hydrocarbon tail where the van der Waals' interactions between the tails provide a robust protective surface layer. The chain terminus can be used to functionalize the SAMs.

In particular, long-chain carboxylic acids have been used as so-called boundary lubricants $^{20-24}$ in which self-assembled monolayers prevent adhesion between the contacting interfaces, thereby lowering friction. 25 These carboxylic acids can also react during sliding to form low-friction carbonaceous layers $^{26-29}$ as exemplified by the reaction of functionalized fatty acids such as elaidic or oleic acid $^{26-30}$ with tetrahedral amorphous carbon. 31 Molecular dynamic (MD) simulations of this process using shorter-chain (2) analogs of these carboxylic acids that contain vinyl groups at various positions in the chain suggest that, because of their bifunctionality, they can simultaneously bind to

Department of Chemistry and Biochemistry, University of Wisconsin-Milwaukee, Milwaukee, WI 53211, USA. E-mail: wtt@uwm.edu

both faces of the contact. This causes very high forces to be exerted on the linked molecule to induce it to tribochemically decompose. Of particular interest is that the cis and trans conformations of these carboxylic acids show different tribochemical activities, presumably because of steric constraints.31 As a precursor to studying the tribochemical surface chemistry and the influence of chain functionalization on reactivity, we first investigate the thermal chemistry and reaction pathways of functionalized carboxylic acids. Rather than studying the chemistry on tetrahedral amorphous carbon, we use a copper substrate, where acetic acid has been shown previously to react to form η^2 -carboxylate species^{32,33} with the methyl-carboxylate bond being close to normal to the surface.³⁴ Acetic acid thermally decomposes on copper with the acetate group first tilting towards the surface and reacting to form adsorbed methyl species and evolve carbon dioxide gas. The tribochemical reaction has been shown to predominantly occur by this route, but a portion can react via an alternative pathway in which the sliding direction changes the molecular tilt to tribochemically form methyl(ads), oxygen(ads), and gas phase carbon monoxide *via* an η^{1} -intermediate.³⁴

Some work has been carried out previously on carboxylic acids adsorbed on copper. Near-edge X-ray adsorption spectroscopy (NEXAFS) has been used to investigate the adsorption of a range carboxylic acids on Cu(111), where the structure was found to depend on the chain length.^{35,36} The deprotonation kinetics of carboxylic acids on copper have been investigated by using fluorine-modified chains,³⁷ and studies of the decomposition of

 $[\]dagger$ Electronic supplementary information (ESI) available. See DOI: 10.1039/d1cp00167a

isotopically labeled carboxylic acids have shown that the reaction is initiated by the removal of carbon dioxide from the carboxylate group.38

The following investigates the adsorption of a medium-chainlength carboxylic acid with a terminal vinyl group, 7-octenoic acid, on a cleaned and annealed copper foil. The molecule is sufficiently small that the vapor pressure is high enough that it can be sublimed in ultrahigh vacuum (UHV), while still being long enough to qualify as a self-assembling system. Copper foils, rather than a single crystal, are chosen as the substrate because tribological experiments will subsequently be carried out on this sample. This causes surface damage so that the use of single crystals is prohibitively expensive. However, it has been shown that these cleaned and vacuum annealed copper foils exhibit sufficient order to display distinct (100) low-energy electron diffraction (LEED) patterns.39 The terminal C=C group will subsequently be modified to test the influence of the terminal functionality of the tribochemical reactivity. The adsorbate structure of the monolayer and multilayer of 7-octenoic acid on copper is studied using a combination of reflection-absorption infrared spectroscopy (RAIRS), X-ray photoelectron spectroscopy (XPS), temperature-programmed desorption (TPD) and scanning tunneling microscopy (STM). The analysis of the results is facilitated using first-principle density functional theory (DFT) calculations.

2. Experimental methods

Experiments were carried out in UHV chambers operating at base pressures of $\sim 2.0 \times 10^{-10}$ torr after bakeout. Infrared spectra were collected using a Bruker Vertex 70 infrared spectrometer using a liquid-nitrogen-cooled, mercury cadmium telluride detector.40 The complete light path was enclosed and purged with dry, CO2-free air and spectra were collected for 1000 scans at 4 cm⁻¹ resolution. Temperature-dependent infrared experiments were performed by precisely controlling the sample temperature by regulating the sample heating current from a Kepco model ATE 6-50M DC power supply using a homemade Labview program interfaced to a National Instruments card (Model USB-6001). The temperature was monitored by means of a chromel/alumel thermocouple spot-welded to the edge of the copper foil, which enabled the sample temperature to be accurately controlled. The effective heating rate for these experiments was $\sim 0.08 \text{ K s}^{-1}$ and enabled infrared spectra to be collected continuously under almost isothermal conditions. TPD experiments were carried out using a Dycor M200M quadrupole mass spectrometer encased with a metal shield to prevent signals from background gases from entering the ionizer, and the end of the shield was placed in close proximity to the front of the copper foil. The foil was dosed using various exposures of 7-octenoic acid at 300 K and the temperature was ramped at a rate of 5 K $\rm s^{-1}$ for each experiment. 7-Octenoic acid coverages were measured from carbon/copper peak-to-peak ratios in Auger electron spectroscopy (AES).

The copper foil sample was prepared by mechanically polishing using sandpapers of increasingly fine grit until reasonably flat.

This was followed by polishing using polycrystalline diamond paste in descending size until 1 µm. This resulted in a visibly smooth surface under a microscope. The sample was mounted in UHV to a precision x, y, z, φ manipulator and cleaned using a standard procedure that consisted of Ar⁺ bombardment with subsequent annealing to 850 K for 10 minutes. Bombardment was performed at a background gas pressure of $\sim 3.0 \times 10^{-5}$ torr of argon at a 2 kV potential while maintaining a ~2 μA sample current. This process was repeated until the sample was determined to be sufficiently clean by AES where, in particular, no carbon or oxygen were detected on the surface. The Cu(100) single crystal used in the STM experiments was cleaned by Ar⁺ bombardment for 30 minutes. This was followed by annealing at 875 K for 30 minutes. This cleaning procedure was repeated until the sample was found to be clean by AES.

7-Octenoic acid (Sigma-Aldrich Chemicals, 97% purity) was purified using several freeze-pump-thaw cycles and its cleanliness was judged by mass spectroscopy and was dosed using a Knudsen source with an attached tube of 3.2 mm internal diameter placed in close proximity to the front of the sample. This arrangement limits the contamination of other parts of the UHV chamber and enhances the local pressure close to the sample. An enhancement factor of 100 was applied to calculate all exposures in the RAIRS chambers and are reported in Langmuirs (1 L = 1×10^{-6} torr s) and were not corrected for ionization gauge sensitivities.

The 7-octenoic acid IR vibrational frequencies were calculated using periodic density functional theory (DFT) using the projector augmented wave (PAW) method as implemented in the Vienna ab initio simulation package (VASP) code.41-43 The exchange and correlation energies were calculated using the PBE (Perdew, Burke and Ernzerhof⁴⁴) form of the generalized gradient approximation (GGA). The kinetic energy cutoff for all calculations was 400 eV. The wavefunctions and electron density were converged to within 1×10^{-5} eV, whereas geometric structures were optimized until the forces on the atoms were less than 0.01 eV \mathring{A}^{-1} . Van der Waals' interactions were implemented using the DFT-D3 method as described Grimme et al. 45 The Brillouin zone was sampled using a Γ -centered Monkhorst-Pack $(1 \times 1 \times 1)$ k-point mesh for gasphase calculations. The gas-phase molecule was first allowed to relax in a sufficiently large cell (36 \times 36 \times 36 Å). For surface calculations, the surfaces consisted of a 5-layer thick 2×2 , 4×4 , and 6 \times 6 Cu(100) slabs with Γ -centered Monkhorst-Pack $(6 \times 6 \times 1)$, $(3 \times 3 \times 1)$, $(2 \times 2 \times 1)$ k-point meshes, respectively. The surfaces were separated by 29 Å and the bottom two copper layers were kept frozen for all calculations. The Cu(100) lattice constant used was 3.63 Å. The normal modes and displacements are displayed using imaging software Vesta.46

3. Results

RAIRS experiments were first carried out by adsorbing 7-octenoic acid on a polished copper foil at 90 K as a function of exposure, and the results are displayed in Fig. 1A. The experimental vibrational frequencies are summarized in Table 1 and are compared with the results of the calculations. The normal modes are

depicted in the ESI† (Fig. S1) and all calculated vibrational frequencies are summarized in Table S1 (ESI†). At very low exposures (0.2 and 1.0 L, Fig. 1A) a single vibrational mode is evident at ~ 1416 cm⁻¹, which is assigned to the in-plane O-H bending vibration of the carboxylic acid group, 47 indicating that the acid functionality remains intact at low coverages and temperatures on copper. As the exposure increases to ~ 2 L, additional peaks appear at 2930 and 2956 cm⁻¹ due to methylene stretches, at 1711 cm⁻¹ due to the C=O stretching mode of the carboxylic acid, along with the associated out-of-plane O-H mode at 915 cm⁻¹, as well as some weak methylene modes at around 970 cm⁻¹. The infrared peaks intensify with increasing exposure where the newly appearing C-H stretching modes are the remaining skeletal vibrations⁴⁸ as indicated in Table 1. As the exposure exceeds \sim 7 L, a broad feature is detected between \sim 2500 and $\sim 3500 \text{ cm}^{-1}$, shown more clearly in the ESI† (Fig. S3), due to the formation of hydrogen-bonded carboxylic acid dimers.⁴⁹ Note that the continued presence of COOH modes throughout the exposure range indicates that 7-octenoic acids adsorbs intact on copper at 90 K.

The integrated absorbances of the carbonyl vibration $(\sim 1711 \text{ cm}^{-1})$ and the skeletal C-H stretching mode $(\sim 2930 \text{ cm}^{-1})$ are plotted as a function of exposure in Fig. 1B. Both vary approximately linearly up to a \sim 55 L exposure and tend to saturate as the film becomes thicker. Since the sticking probability is unlikely to change at this adsorption temperature, a possible explanation for this observation is that the 7-octanoic acid film is sufficiently thick at this exposure that the infrared beam has

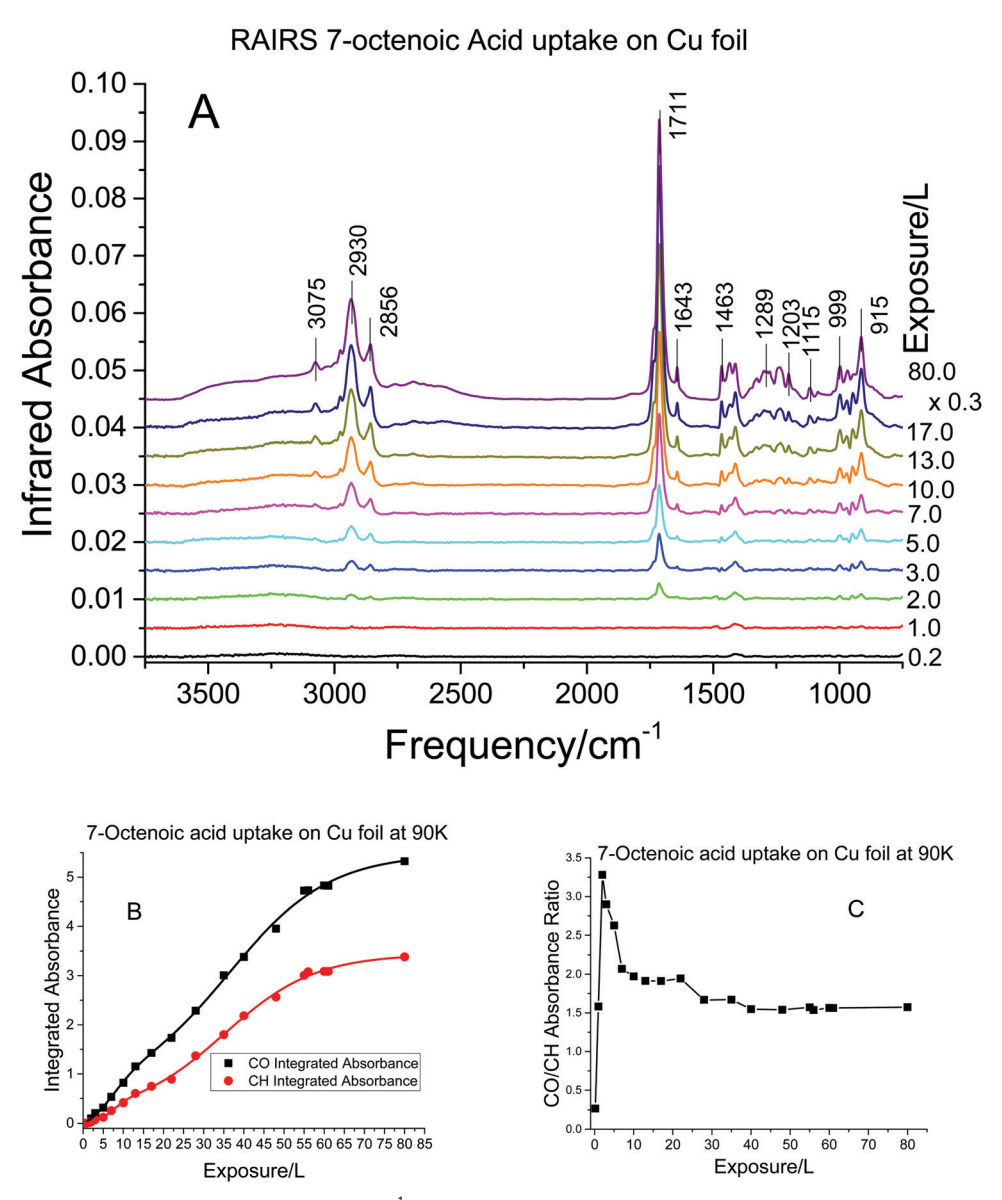


Fig. 1 (A) Infrared spectra collected using a resolution of 4 cm⁻¹ for the adsorption of 7-octenoic acid on Cu(100) at a sample temperature of 90 K as a function of exposure on Langmuirs (L), where the exposures are displaced adjacent to the corresponding spectrum. (B) Plot of the integrated absorbances for the carbonyl mode (CO vibration at \sim 1711 cm⁻¹) and the C-H stretching vibrations (CH vibrations at \sim 2930 cm⁻¹) and as function of the 7-octenoic acid exposure and (C) the ratio of the integrated absorbances of the CO and CH modes as a function of exposure, in Langmuirs (L).

Table 1 Assignments of the vibrational spectra of 7-octenoic acid on copper

Mode number	Calculated frequency/cm ⁻¹	7-Octenoic acid multilayer/Cu(100)/cm ⁻¹	7-Octenoic acid annealed multilayer/Cu(100)/cm ⁻¹	Assignments
1	3529	3500-2900 broad	3075	O-H stretch
2	2955	2975	2975	CH ₂ asymmetric stretch
4, 5	2937, 2914	2929	2930	CH ₂ asymmetric stretch
11, 15, 16	2878, 2858, 2854	2856	2856	CH ₂ symmetric stretch
17	1708	1716	1713	C=O stretch
18	1422	1471	1468, 1434	CH ₂ scissor
20	1414	1412	1416	In-plane O–H bend
27	1326	1327		CH ₂ scissor
30	1278	1286	1289	C-O stretch
34	1239	1242	1238	CH ₂ twist/wag
36	1205	1203	1200	CH ₂ twist/wag
39	1141	1116	1120	C-C stretch
47	976	966	970	CH ₂ rock
48	958		939	C–H modes
			515	Out-of-plane O-H bend

been attenuated. The most intense 1711 cm $^{-1}$ feature has a peak absorbance of ~ 0.55 after an 80 L exposure. However, more subtle variations are evident when plotting the absorbance ratio of the carbonyl and CH $_2$ vibrations (Fig. 1C). Here the ratio varies rapidly for the first few Langmuirs exposure from ~ 0.2 at a low exposure to ~ 3.2 at an exposure of ~ 5 L. The ratio then decreases slowly with increasing exposure to plateau at a value of ~ 1.5 for exposures greater than 30 L.

The effect of heating the 7-octenoic acid multilayer is shown in Fig. 2, where the annealing temperatures are displayed adjacent to the corresponding spectra. The positions of the peaks remain unchanged as the sample is heated, although the spectra become significantly sharper beginning at 160 K, in particular for the region between 1100 and 1500 cm⁻¹. These modes are due mainly to skeletal methylene vibrations and indicate that the multilayer becomes more ordered. Annealing to 190 K causes the integrated absorbance of carbonyl stretching mode to increase very slightly (by 8.3%), while its peak absorbance increases much more (by 41.2%). This narrowing of the carbonyl mode and the accompanied disappearance of the broad OH feature between $\sim 2500-3500~\text{cm}^{-1}$ indicate that the dimer has dissociated. The integrated intensities of the carbonyl and C-H stretching vibrations remain unchanged on heating to ~200 K, but then decrease rapidly at higher temperatures due to multilayer desorption. The significantly attenuated spectrum remaining at 265 K (Fig. 1A) has vibrational frequencies that are similar to the multilayer, except with different relative intensities. In particular, the C-O stretching (1288 cm⁻¹) and O-H bending (1413 and 915 cm⁻¹) modes are still present, implying that the 7-octenoic acid remains intact at this temperature. The intense O-H stretching mode centered at 3190 cm⁻¹ is significantly narrower than for the multilayer, indicating that 7-octenoic acid is mainly present as a monomer and has not yet deprotonated.

To investigate the behavior when adsorbing 7-octenoic acid at 300 K, the infrared spectra are displayed in Fig. 3A. The most intense peak is due to the carboxylate COO symmetric stretching mode, which shifts from $\sim 1408~{\rm cm}^{-1}$ at low exposures to $\sim 1425~{\rm cm}^{-1}$ at saturation. The intensity variation of the

COO (\blacktriangle) and CH₂ stretching modes (\blacksquare , \bullet) are plotted *versus* exposure in Fig. 3B, and the CO/CH absorbance ratios are plotted *versus* exposure in Fig. 3C. The observed variation suggests that there is a change in molecular orientation as the exposure increases to \sim 2 L. The C \equiv O vibrational mode at saturation (1425 cm $^{-1}$) is close to that found for acetate species on Cu(100)³² and is different from that for the 7-octenoic acid multilayer. To confirm that carboxylate species are present following adsorption at 300 K, the O 1s XPS spectrum for a saturated overlayer is shown in Fig. 4, showing a peak centered at 532.5 eV binding energy, close to that found for carboxylate species on Cu(111).³⁶

The effect on the infrared spectra of heating the 7-octenoic-acid covered sample is documented in Fig. 5A, which shows mainly the most intense carbonyl vibration at $\sim\!1425~{\rm cm}^{-1}$ due to adsorbed carboxylate species. This remains reasonably constant in intensity and frequency on heating to $\sim\!344~{\rm K}$, then starts to decrease in intensity and shift to a slightly lower frequency ($\sim\!1406~{\rm cm}^{-1}$) at 392 K and above. This is accompanied by the appearance of a peak at $\sim\!1485~{\rm cm}^{-1}$ due to an asymmetric carboxylate COO stretching mode. This indicates that the plane of that carboxylate group is initially oriented perpendicularly to the surface, but tilts towards the surface at 392 K and higher temperatures.

In order to compare the infrared spectroscopic changes with the desorption products, TPD measurements were made to monitor 44 (carbon dioxide) and 2 amu (hydrogen) to detect hydrocarbon decomposition products. The results are displayed in Fig. 5B and C using a heating rate of 5 K s⁻¹, much higher than the effective heating rate used for the infrared experiments of 0.08 K s⁻¹. The relative coverages were determined from the AES C/Cu peak-to-peak ratios and compared with the value for the saturated overlayer. The majority of the carbon dioxide desorbs in a broad peak centered at ~650 K, which grows in intensity as the 7-octenoic acid coverage increases (Fig. 5B). The coverage at which this state saturates is taken to correspond to 1 monolayer (ML) of 7-octenoate species. At lower coverages, CO₂ desorbs in an additional state centered at 550 K which shifts to higher temperatures and attenuates at a coverage of 0.27 ML. The 2 amu TPD results (Fig. 5C) show that at 0.21 ML the **PCCP**

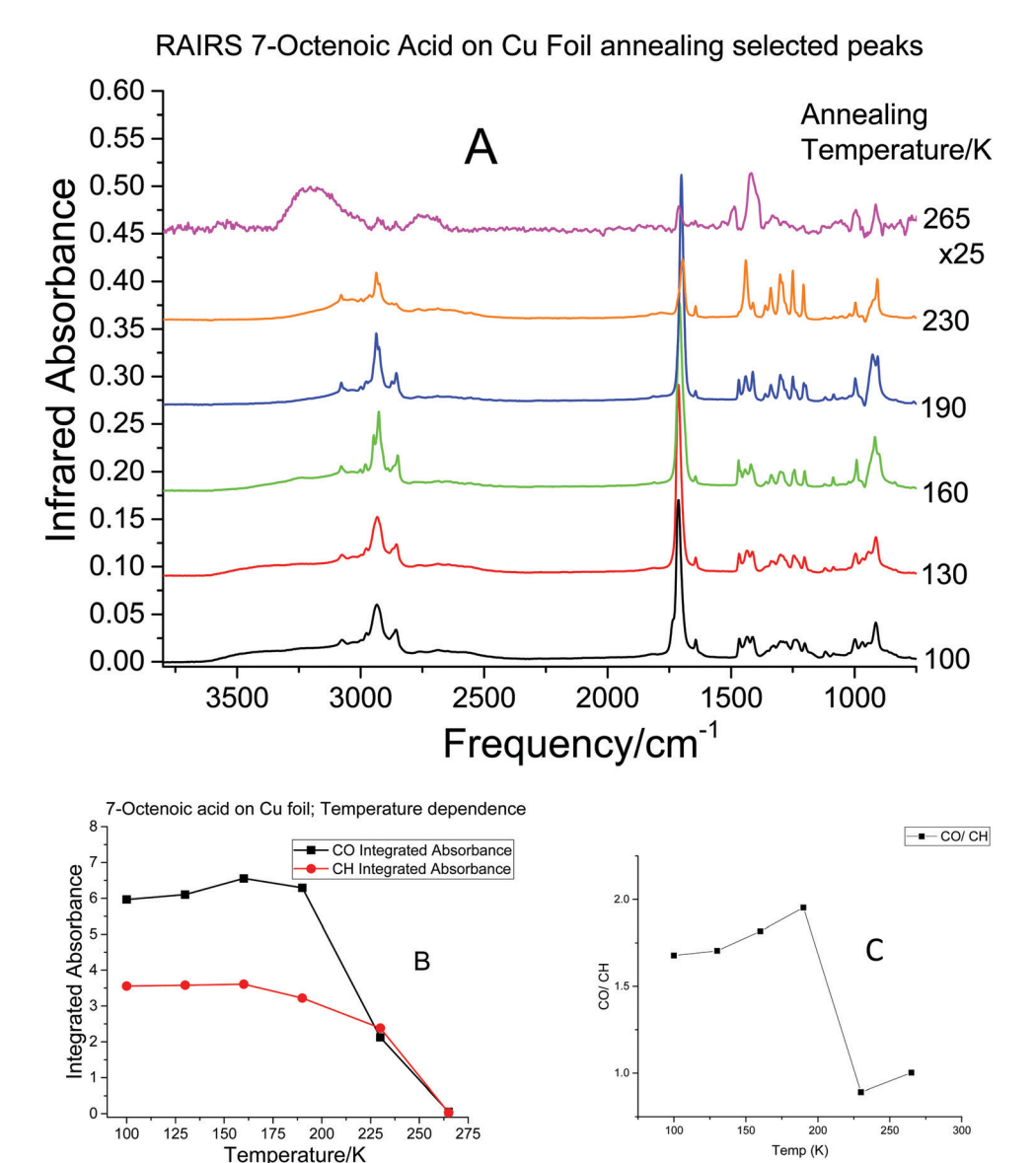


Fig. 2 (A) Infrared spectra collected using a resolution of 4 cm⁻¹ for the adsorption of 7-octenoic acid on Cu(100) at a sample temperature of 90 K heated to various temperatures, where the temperatures are displaced adjacent to the corresponding spectrum. (B) Plot of the integrated absorbances for the carbonyl mode (CO vibration at \sim 1711 cm⁻¹) and the C-H stretching vibrations (CH vibrations at \sim 2930 cm⁻¹) and as function of annealing temperature. (C) The ratio of the integrated absorbances of the CO and CH modes as a function of temperature, in Kelvin (K)

hydrogen desorption signal intensity is minimal, but still present, with a broad peak centered at 700 K. As the surface coverage increases above 0.27 ML, a relatively sharp hydrogen desorption peak appears centered at 615 K, when only a small amount of CO₂ is formed. The formation of CO_2 at ~ 650 K is accompanied by the desorption of hydrogen, while a final broad 2 amu desorption state is seen at \sim 740 K when CO_2 evolution is complete.

The evolution in surface structure is shown in the STM images in Fig. 6 and 7 where chain-like carbonaceous species are evident after heating to 600 K (Fig. 6A). This reveals a series of protrusions that are a few Angstroms apart, but with a variety of lengths perpendicular to the surface, mainly corresponding to the presence of chains tilted at various angles with respect to the surface proposed to presage the onset of hydrogen formation in TPD experiments.

The nature of the surface changes completely at 700 K (Fig. 6B) and consists of large, string-like patches, while the TPD data suggest that surface still contain some hydrogen (Fig. 5B). These features extend over several nanometers and are therefore assigned to the formation of polymeric species. A close-up of this surface (Fig. 6C) reveals large macrocyclic regions as well as remaining polymeric species. Heating to 850 K (Fig. 6D-F), when decarboxylation is complete, reveals that polymeric species are still apparent, but there is evidence that some can react to form nanoscale carbonaceous films by cohering into islands with flat terraces. This appears to occur by the polymers diffusing to form islands on flat regions on the substrate as indicated by the blue arrows in Fig. 6D or to move to forms flat regions that decorate step edges as indicated in Fig. 6E. Some species are still present as

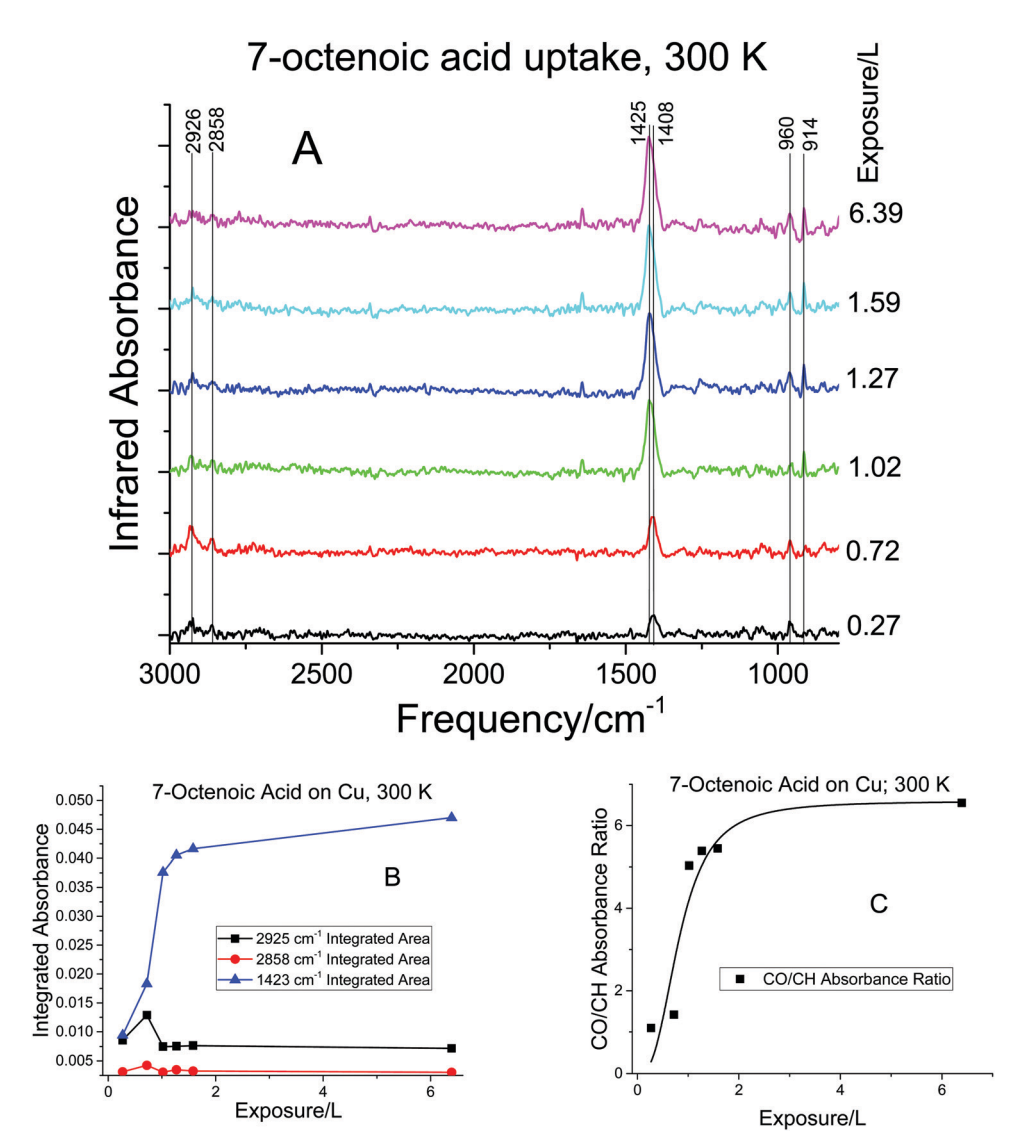


Fig. 3 (A) Infrared spectra collected using a resolution of $4 \, \mathrm{cm}^{-1}$ for the adsorption of 7-octenoic acid on Cu(100) at a sample temperature of 300 K as a function of exposure in Langmuirs (L), where the exposures are displaced adjacent to the corresponding spectrum. (B) Plot of the integrated absorbances for the carbonyl mode (CO vibration at $\sim 1711 \, \mathrm{cm}^{-1}$) and the C–H stretching vibrations (CH vibrations at $\sim 2930 \, \mathrm{cm}^{-1}$) and as function of the 7-octenoic acid exposure and (C) the ratio of the integrated absorbances of the CO and CH modes as a function of exposure, in Langmuirs (L).

polymeric formations as shown by the light blue circle in Fig. 6D. Additional small, circular features are observed (circled in white in Fig. 6E) that can also initiate the formation of small isolated clusters.

The effect of heating to ~ 1000 K is shown in Fig. 7A and B. The cohering and subsequent reaction of polymeric species into carbonaceous agglomerates is complete by this temperature. Several defects are present in the overlayers after they have formed, indicating that they are sufficiently stable not to be able to undergo further ordering at this temperature. These defects are present as low-coordination sites and as holes that decorate the terrace surface. It can also be seen that the carbonaceous overlayer is not only due to a single, graphene-like monolayer, but can also form additional graphitic multilayers. As seen in Fig. 7C and D, the overlayer does exhibit some graphitic rings, but has many defective areas and low order.

4. Discussion

DFT calculations were carried out to investigate the structure and stability of 7-octenoate species on a Cu(100) substrate to aid in interpreting the experimental data. The results are shown in Fig. 8 and 9. Fig. 8 shows a flat-lying configuration formed at low coverages with the C_7 chain oriented close to parallel to the surface. Here, the terminal vinyl group binds to the surface due to the interaction between the π -orbitals and the copper substrate. This causes the OCO group to tilt with respect to the surface to allow the chain to interact with the copper, leading to a binding energy of 411 kJ mol $^{-1}$. The geometries of the more vertical 7-octenoate species are shown in Fig. 9. The size of the unit cell used for this calculation is changed to vary the coverage. In all cases, the molecule binds with the plane of the carboxylate anchoring group perpendicular to the surface with the chain

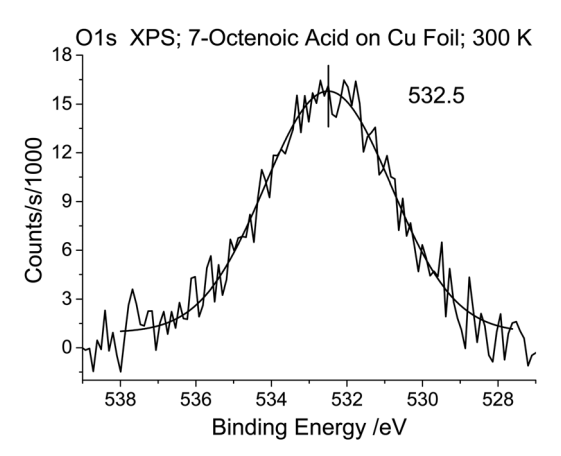


Fig. 4 Oxygen 1s Mg K α X-ray photoelectron spectrum collected using a pass energy of 50 eV for the adsorption of 7-octenoic acid on Cu(100) at a sample temperature of 300 K.

tilted at $\sim 50^\circ$. An inspection of the optimized structure of the vertical species on copper indicates that the terminal vinyl group is oriented in such a way that the C=C functionality faces away from the surface to allow the π -orbitals to easily access an approaching counterface. The depictions in Fig. 9 also indicate that the orientation of the terminal group will depend on the number of methylene groups on the chain. Note that the

interaction between the termini of the anchored carboxylic acid and the counterface has been proposed to influence the rate of tribochemical decomposition. Since the resulting carboxylates are thermally stable on copper up to ~ 500 K (Fig. 5), this provides an ideal system for studying such effects.

The DFT results on various slabs enable the binding energy to be calculated as a function of coverage (Fig. 9D), which varies from $\sim\!350~\rm kJ~\rm mol^{-1}$ at low coverages, stabilizing by $\sim\!30~\rm kJ~\rm mol^{-1}$ as the coverage increase to 0.25 ML, due to the intermolecular van der Waals' interactions. A desorption temperature of $\sim\!1300$ to 1440 K can be estimated for this binding energy using the experimental heating rate of 5 K s $^{-1}$ and assuming a typical pre-exponential factor of 1 \times 10 13 s $^{-1}$. This is much higher than the decomposition temperature range of $\sim\!550$ to 800 K (Fig. 5), indicating that long-chain fatty acids are strongly anchored to the copper surface.

7-Octenoic acid adsorbs molecularly on a copper substrate when the temperature is below ~ 265 K (Fig. 2), where the molecular orientation depends on coverage. At low coverages, the molecule adsorbs with the chain close to parallel to the surface, either at 90 K (Fig. 1C) or at room temperature (Fig. 2C) in a geometry that is analogous to the striped phases of long-chain thiols on gold imaged by STM. 2,50 As the coverage increases and the surface becomes more crowded, the orientation changes to form more upright chains that are stabilized due to the interchain Van der Waals' interactions of ~ 4 kJ mol $^{-1}$ per methylene group

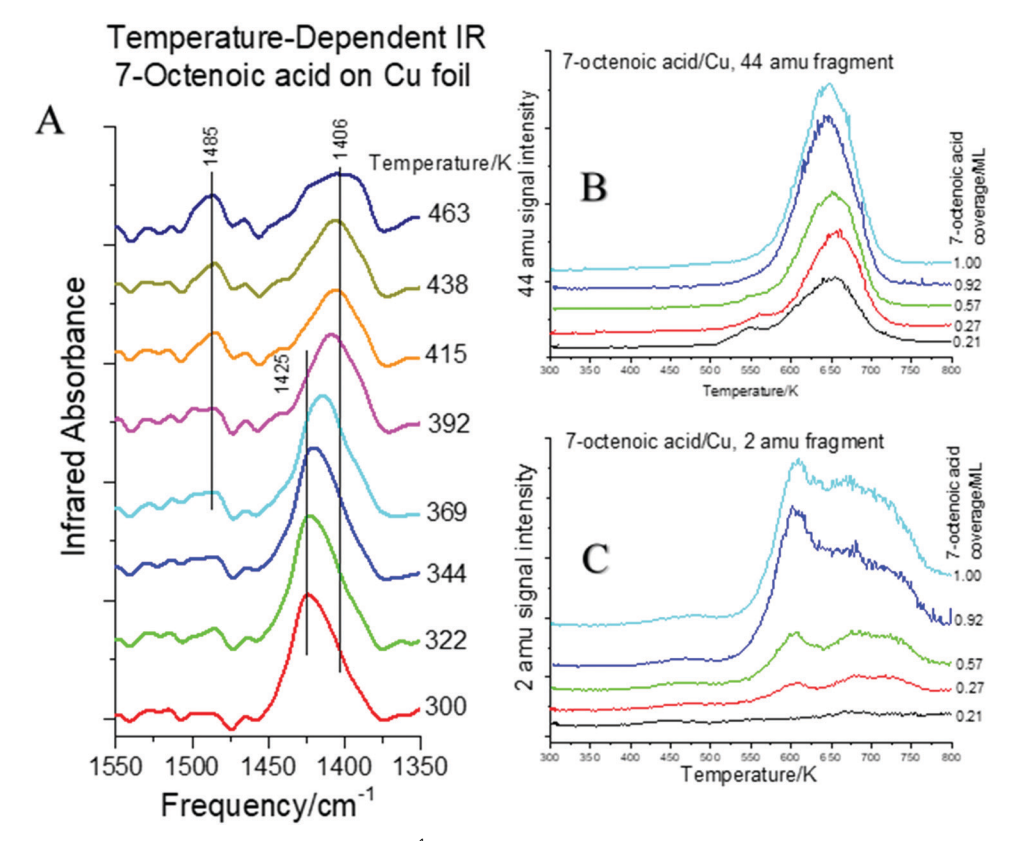


Fig. 5 (A) Infrared spectra collected using a resolution of 4 cm $^{-1}$ for the adsorption of 7-octenoic acid on Cu(100) at a sample temperature of 300 K heated to various temperatures, where the temperatures are displaced adjacent to the corresponding spectrum. (B) Temperature-programmed desorption (TPD) for the adsorption of 7-octenoic acid on Cu(100) at a sample temperature of 300 K as a function of 7-octenoic coverage using a heating rate of 5 K s $^{-1}$ while monitoring (B) 44 and (C) 2 amu, where coverages are displaced adjacent to the corresponding spectrum.

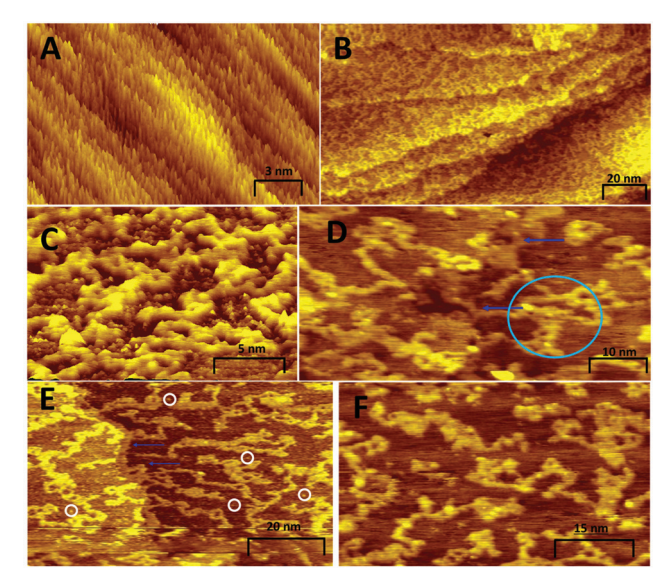


Fig. 6 Scanning tunneling microscope (STM) images of a saturated overlayer of 7-octenoic acid adsorbed at 300 K on Cu(100). (A) 20 nm \times 15 nm image after heating to 600 K ($V_b = -0.76$ V, $I_t = 0.109$ nA), (B) 19 nm \times 13 nm image after heating to 700 K ($V_b = -0.75 \text{ V}$, $I_t = 0.100 \text{ nA}$) and (C) 80 nm \times 45 nm image ($V_b = -0.75 \text{ V}$, $I_t = 0.094 \text{ nA}$) image after heating to 850 K, (D) 60 nm \times 35 nm image ($V_b = -0.76 \text{ V}$, $I_t = 0.097 \text{ nA}$), (E) 80 nm \times 45 nm image $(V_{\rm b} = -0.76 \text{ V}, I_{\rm t} = 0.099 \text{ nA}), \text{ and (F) } 60 \text{ nm} \times 35 \text{ nm image } (V_{\rm b} = -0.76 \text{ V},$ $I_{\rm t}$ = 0.097 nA) after heating to 850 K.

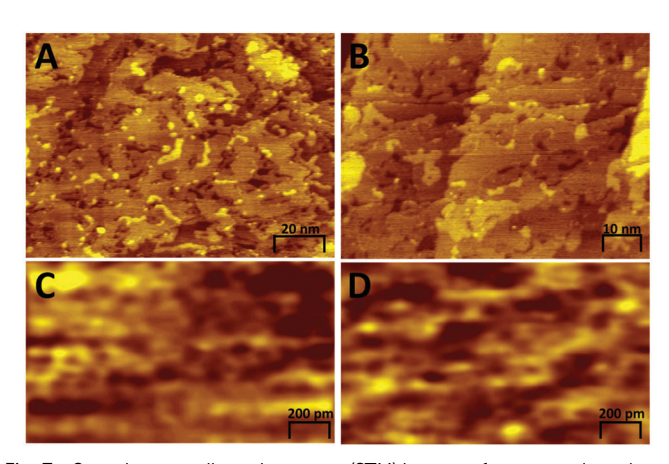


Fig. 7 Scanning tunneling microscope (STM) images of a saturated overlayer of 7-octenoic acid adsorbed at 300 K on Cu(100). (A) 150 nm \times 120 nm image after heating to 1000 K ($V_{\rm b}$ = -0.76 V, $I_{\rm t}$ = 0.102 nA), (B) 70 nm imes 50 nm image after heating to 1000 K ($V_{\rm b}$ = -0.76 V, $I_{\rm t}$ = 0.092 nA) and (C) 1.5 nm imes 0.8 nm image ($V_{\rm b}$ = -0.76 V, $I_{\rm t}$ = 0.127 nA) and (D) 1.5 nm imes 0.8 nm image ($V_{\rm b}$ = -0.76 V, $I_{\rm t}$ = 0.127 nA), both after heating to 1000 K.

in the chain.^{51,52} This effect is particularly noticeable for adsorption at 90 K (Fig. 1C), where there is a sharp transition in the ratio of the absorbances of the carbonyl and methylene stretching modes, consistent with molecular reorientation to form a chain that is close to perpendicular to the surface. As the coverage increases, this ratio tends to a lower value (of ~ 1.5), due to the formation of a condensed 7-octenoic acid film with randomly ordered molecules. Similar behavior is seen for the adsorption of

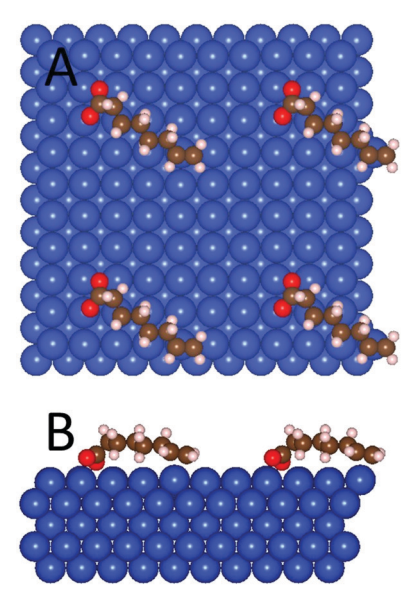


Fig. 8 Most-stable structure of flat-lying 7-octenoic acid on Cu(100) calculated by density functional theory showing (A) a top view and (B) a side view.

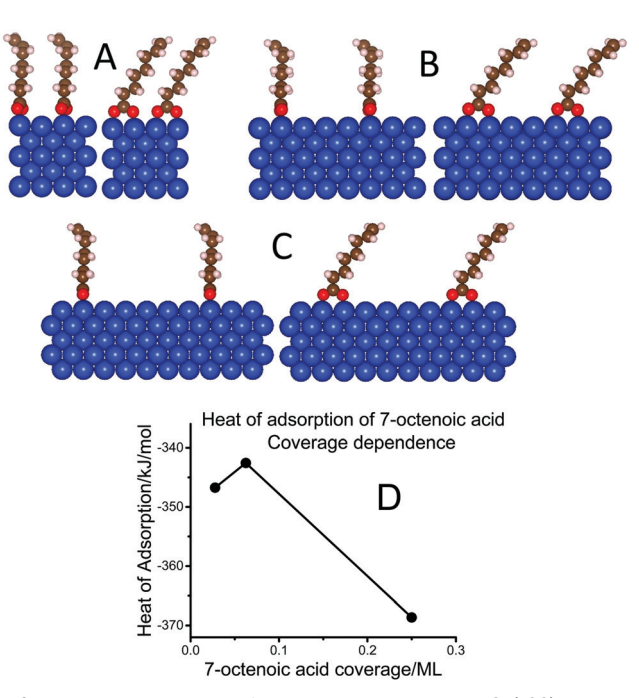


Fig. 9 Most-stable structure of vertical 7-octenoic acid on Cu(100) calculated by density functional theory showing (A) a 2 \times 2, (B) a 4 \times 4 and (C) a 6 \times 6 overlayer, and figure (D) shows the heat of adsorption of 7-octenoic acid as a function of coverage.

7-octenoic acid at 300 K (Fig. 3C), where there is an analogous increase in the ratio of the CO and CH mode absorbances, which reaches a value of ~6 for adsorption at 300 K compared to a maximum of \sim 3.8 for adsorption at 90 K. This is presumably due to the larger chain mobility at higher temperatures that allows it to form a more ordered SAM. This effect is also seen in Fig. 2 where

the vibrational modes become sharper as the 7-octenoic overlayer is heated to ~230 K. Condensed 7-octenoic acid desorbs at ~225 K (Fig. 2B) leaving behind an adsorbed molecular layer when the sample has been heated to 265 K (note the expanded absorbance scale).

Adsorbed 7-octenoic acid deprotonates on copper at 300 K and the shift in the C=O vibrational frequency from 1711 cm⁻¹ for molecular 7-octenoic acid (Fig. 1) to the 7-octenoate at 1425 cm⁻¹ (Fig. 3) is relatively modest. Deprotonation is confirmed by the O 1s photoelectron spectrum (Fig. 4) from the binding energy, which is consistent with the formation of a carboxylate species on copper, while the presence of a single O 1s peak indicates that the two oxygen atoms are chemically equivalent and is assigned to an η^2 -carboxylate. The splitting between $\nu(COO)$ symmetric and asymmetric modes of approximately 80 cm⁻¹ is characteristic of a bidentate bounded carboxylate.53

The adsorbed 7-octenoate species decomposes in a similar manner as found for acetic acid,⁵⁴ by the COO plane tilting towards the surface to induce C-CH2 bond scission to evolve CO2 that originates from the carboxylate group as shown in Fig. 8 to allow the hydrocarbon chain access to the surface, and may be assisted by the interaction of the terminal vinyl group with the surface. Further evidence for the carboxylate tilting comes from the infrared spectra in Fig. 5A, which show an increase in relative intensity of the of the asymmetric COO mode at 1485 cm⁻¹ at higher temperatures, and a shift of the symmetric COO stretch from 1425 to 1408 cm⁻¹ as the oxygen-surface binding changes. The ability of the adsorbate to tilt will depend on its initial coverage and are suggested to form tilted species at lower coverages. The small 44 amu feature centered at \sim 550 K (Fig. 5B) is attributed to the decomposition of a flat-lying species present that facilitates decarbonylation to reduce the CO2 desorption temperature. This species can also dehydrogenate as evidenced by the detection of hydrogen at \sim 530 K (Fig. 5C), this feature attenuates and moves to higher temperature as the coverage increases in accord with this picture. Decarbonylation of more closely packed overlayers occurs at higher temperatures and gives rise to CO2 evolution at 650 K.

After decarboxylation, the resulting carbonaceous species can react to form hydrocarbons by β-hydride elimination, or undergo coupling reactions^{55–57} to deposit oligomeric species on the surface (Fig. 6). While β-hydride elimination is the dominant decomposition pathway for alkyl species on copper, they can undergo other, dehydrogenation reaction pathways when formed at higher temperatures, by decarbonylation. Hydrogens is first formed at ~615 K (Fig. 5C) prior to any significant CO₂ production (Fig. 5B) and may be due to the 7-octenoate tilting to allow it to dehydrogenate (Fig. 8B) as suggested by the infrared data (Fig. 5A). Hydrogen is produced coincident with CO₂ evolution, but a significant amount is also formed after this is complete. This suggests that a significant amount of carbonaceous species remain on the surface. This is confirmed by the STM images found after heating to ~700 K (Fig. 6A), which show that there are hydrocarbons on the surface with a significant variation in chain length. This implies that, once the reaction has been initiated, it provides space to facilitate the tilting of other molecules to allow the reaction to accelerate as well as to polymerize by reacting with neighboring chains. This leads to change in selectivity towards hydrogen formation compared to the CO₂ yield of the decomposition reaction as a function of coverage, where only a small amount of hydrogen is formed at low coverages, while more dehydrogenation takes place as the 7-octenoic acid coverage increases (Fig. 5C).

The adsorbate has almost completely decarbonylated at \sim 700 K and the production of CO2 has almost ceased (Fig. 5B). However, the remaining carbonaceous species still contain a significant amount of hydrogen (Fig. 5C). There are no longer any vertical adsorbates and the surface consists of carbonaceous patches (Fig. 6B). Heating to 850 K removes more hydrogen and produces larger patches of rather disordered carbonaceous deposits (Fig. 6C and D) and form assemblies that consist of small circular entities that can cluster together to produce larger patches. Fig. S2 (ESI†) compares the C/Cu ratio determined by AES before dosing 7-octenoic acid, after saturation exposure, and after annealing the saturated surface to 850 K. This shows that the remaining surface species at 850 K contains approximately 47% of the carbon present in the saturated overlayer. No other AES peaks, particularly those due to oxygen, are detected after annealing to 850 K. Heating to higher temperatures (~ 1000 K, Fig. 7) leads to carbonaceous regions that show a hexagonal motif at higher magnification consistent with the onset of formation of a poorly ordered graphene layer.⁵⁸

Finally, the presence of unsaturation in the carbonaceous chain is also likely to influence the way in which the adsorbed carboxylate-anchored SAMs react with the surface. The presence of unsaturation is therefore likely produce a more reactive film than SAMs formed from saturated hydrocarbons. Such effects are also likely to influence the tribo/mechanochemistry as well as the thermal chemistry.

Conclusion

The adsorption structure and reaction pathway of 7-octenoic acid was investigated under UHV conditions on both a polished copper foil and a Cu(100) single crystal using RAIRS, XPS, AES, TPDs, and supported by DFT calculations, as a precursor to tribological studies. 7-Octenoic acid adsorbs molecularly at low temperatures, converting from a flat-lying species at low coverages, to a more vertical species at the coverages increases. It deprotonates upon adsorbing at 300 K and forms bidentate structure, binding to the surface through the carboxylate oxygen atoms. At low coverages, the 7-octenoic acid can form a flat-lying species, but tilts upright as coverage increases. Upon heating, the 7-octenoic acid tilts towards the surface allowing for some dehydrogenation, followed by decarboxylation to evolve CO2. This deposits a C7 fragment that can either dehydrogenate as it is formed, or produce surface oligomers, which accounts for ~47% of the carbon remaining on the surface without any observed remaining oxygen. These oligomeric species continue to dehydrogenate at higher temperatures, finally forming a carbonaceous overlayer.

Conflicts of interest

There are no conflicts to declare.

Acknowledgements

We gratefully acknowledge the Civil, Mechanical and Manufacturing Innovation (CMMI) Division of the National Science Foundation under grant number CMMI-2020525 for support of this work.

References

- 1 D. K. Schwartz, Annu. Rev. Phys. Chem., 2001, 52, 107–137.
- 2 C. Vericat, M. E. Vela and R. C. Salvarezza, *Phys. Chem. Chem. Phys.*, 2005, 7, 3258–3268.
- 3 P. E. Laibinis, G. M. Whitesides, D. L. Allara, Y. T. Tao, A. N. Parikh and R. G. Nuzzo, *J. Am. Chem. Soc.*, 1991, 113, 7152–7167.
- 4 H. Sellers, A. Ulman, Y. Shnidman and J. E. Eilers, *J. Am. Chem. Soc.*, 1993, **115**, 9389–9401.
- 5 A. Ulman, Chem. Rev., 1996, 96, 1533-1554.
- 6 B. M. Rosen and V. Percec, Nature, 2007, 446, 381-382.
- 7 K. G. Thomas and P. V. Kamat, Acc. Chem. Res., 2003, 36, 888–898.
- 8 C. A. Mirkin and M. A. Ratner, Annu. Rev. Phys. Chem., 1992, 43, 719–754.
- 9 S. N. Yaliraki, M. Kemp and M. A. Ratner, *J. Am. Chem. Soc.*, 1999, **121**, 3428–3434.
- 10 J. H. Schon, H. Meng and Z. Bao, Nature, 2001, 413, 713-716.
- 11 D. Olson, A. Boscoboinik, S. Manzi and W. T. Tysoe, J. Phys. Chem. C, 2019, 123, 10398–10405.
- 12 D. Olson, A. Boscoboinik and W. T. Tysoe, *Chem. Commun.*, 2019, 55, 13872–13875.
- 13 K. Komvopoulos, Wear, 1996, 200, 305-327.
- 14 R. Maboudian, W. R. Ashurst and C. Carraro, *Sens. Actuators*, *A*, 2000, **82**, 219–223.
- J. I. Henderson, S. Feng, G. M. Ferrence, T. Bein and C. P. Kubiak, *Inorg. Chim. Acta*, 1996, 242, 115–124.
- 16 T. Ishida, S. i. Yamamoto, W. Mizutani, M. Motomatsu, H. Tokumoto, H. Hokari, H. Azehara and M. Fujihira, *Langmuir*, 1997, 13, 3261–3265.
- 17 S. A. Swanson, R. McClain, K. S. Lovejoy, N. B. Alamdari, J. S. Hamilton and J. C. Scott, *Langmuir*, 2005, 21, 5034–5039.
- 18 N. A. Kautz and S. A. Kandel, *J. Am. Chem. Soc.*, 2008, **130**, 6908–6909.
- 19 D. P. Woodruff, Phys. Chem. Chem. Phys., 2008, 10, 7211-7221.
- 20 D. Clayton, Br. J. Appl. Phys., 1951, 2, 25.
- 21 F. J. Westlake and A. Cameron, *Proceedings of the Institution of Mechanical Engineers, Conference Proceedings*, 1967, vol. 182, pp. 75–78.
- 22 A. Tonck, J. M. Martin, P. Kapsa and J. M. Georges, *Tribol. Int.*, 1979, 12, 209–213.
- 23 S. M. Hsu and R. S. Gates, Tribol. Int., 2005, 38, 305-312.
- 24 H. Spikes, Tribol. Lett., 2015, 60, 5.
- 25 R. Simič and M. Kalin, Appl. Surf. Sci., 2013, 283, 460-470.
- 26 M. Kano, J. M. Martin, K. Yoshida and M. I. De Barros Bouchet, *Friction*, 2014, 2, 156–163.

- 27 M. I. De Barros Bouchet, J. M. Martin, J. Avila, M. Kano, K. Yoshida, T. Tsuruda, S. Bai, Y. Higuchi, N. Ozawa, M. Kubo and M. C. Asensio, *Sci. Rep.*, 2017, 7, 46394.
- 28 M. I. De Barros Bouchet, J. M. Martin, C. Forest, T. le Mogne, M. Mazarin, J. Avila, M. C. Asensio and G. L. Fisher, *RSC Adv.*, 2017, 7, 33120–33131.
- 29 S. Campen, J. H. Green, G. D. Lamb and H. A. Spikes, *Tribol. Lett.*, 2015, 57, 18.
- 30 S. M. Lundgren, M. Ruths, K. Danerlöv and K. Persson, J. Colloid Interface Sci., 2008, 326, 530–536.
- 31 T. Kuwahara, P. A. Romero, S. Makowski, V. Weihnacht, G. Moras and M. Moseler, *Nat. Commun.*, 2019, 10, 151.
- 32 B. A. Sexton, Chem. Phys. Lett., 1979, 65, 469-471.
- 33 M. Bowker and R. J. Madix, Appl. Surf. Sci., 1981, 8, 299-317.
- 34 R. Rana, R. Bavisotto, N. Hopper and W. T. Tysoe, *Tribol. Lett.*, 2021, **69**, 32.
- 35 D. Fuhrmann, D. Wacker, K. Weiss, K. Hermann, M. Witko and C. Woll, *J. Chem. Phys.*, 1998, **108**, 2651–2658.
- 36 M. Wühn, J. Weckesser and C. Wöll, *Langmuir*, 2001, **17**, 7605–7612.
- 37 B. Immaraporn, P. Ye and A. J. Gellman, *J. Phys. Chem. B*, 2004, **108**, 3504–3511.
- B. Karagoz, A. Reinicker and A. J. Gellman, *Langmuir*, 2019,
 35, 2925–2933.
- 39 O. J. Furlong, B. P. Miller, Z. Li, J. Walker, L. Burkholder and W. T. Tysoe, *Langmuir*, 2010, **26**, 16375–16380.
- 40 M. Kaltchev, A. W. Thompson and W. T. Tysoe, *Surf. Sci.*, 1997, **391**, 145–149.
- 41 G. Kresse and J. Hafner, *Phys. Rev. B: Condens. Matter Mater. Phys.*, 1993, 47, 558–561.
- 42 G. Kresse and J. Furthmüller, *Comput. Mater. Sci.*, 1996, 6, 15–50.
- 43 G. Kresse and J. Furthmüller, *Phys. Rev. B: Condens. Matter Mater. Phys.*, 1996, **54**, 11169–11186.
- 44 J. P. Perdew, K. Burke and M. Ernzerhof, *Phys. Rev. Lett.*, 1996, 77, 3865–3868.
- 45 S. Grimme, J. Antony, S. Ehrlich and H. Krieg, *J. Chem. Phys.*, 2010, 132, 154104.
- 46 K. Momma and F. Izumi, *J. Appl. Crystallogr.*, 2011, 44, 1272–1276.
- 47 J.-J. Max and C. Chapados, *J. Phys. Chem. A*, 2004, **108**, 3324–3337.
- 48 M. J. Hostetler, J. J. Stokes and R. W. Murray, *Langmuir*, 1996, **12**, 3604–3612.
- 49 V. Doan, R. Köppe and P. H. Kasai, *J. Am. Chem. Soc.*, 1997, **119**, 9810–9815.
- 50 M. Sharma, M. Komiyama and J. R. Engstrom, *Langmuir*, 2008, 24, 9937–9940.
- 51 T. B. Creczynski-Pasa, M. A. D. Millone, M. L. Munford, V. R. de Lima, T. O. Vieira, G. A. Benitez, A. A. Pasa, R. C. Salvarezza and M. E. Vela, *Phys. Chem. Chem. Phys.*, 2009, 11, 1077–1084.
- 52 E. Torres, A. T. Blumenau and P. U. Biedermann, *Chem-PhysChem*, 2011, **12**, 999–1009.
- 53 K. Nakamoto, *Infrared and Raman spectra of inorganic and coordination compounds*, John Wiley, New York, 1978.

- 54 R. Rana, R. Bavisotto, N. Hopper and W. Tysoe, *Tribol. Lett.*, 5
- 55 C. J. Jenks, C. M. Chiang and B. E. Bent, *J. Am. Chem. Soc.*, 1991, 113, 6308–6309.
- 56 B. E. Bent, Chem. Rev., 1996, 96, 1361-1390.

PCCP

2021, 69, 32.

- 57 C. J. Jenks, B. E. Bent and F. Zaera, *J. Phys. Chem. B*, 2000, **104**, 3017–3027.
- 58 X. S. Li, W. W. Cai, J. H. An, S. Kim, J. Nah, D. X. Yang, R. Piner, A. Velamakanni, I. Jung, E. Tutuc, S. K. Banerjee, L. Colombo and R. S. Ruoff, *Science*, 2009, 324, 1312–1314.